Sensors & Transducers, Vol. 269, Issue 2, July 2025, pp. 22-29

www.sensorsportal.com

Sensors & Transducers

Published by IFSA Publishing, S. L., 2025
http://www.sensorsportal.com

Determining the Effects of Hybrid Analysis Methods on the Reliability of Fringe Projection Profilometry

Burak ÖZBAY and * Zehra SARAÇ
Istanbul Medeniyet University, Department of Electrical and Eectronics Engineering, 34700, Istanbul, Turkey
Tel.: +90 216 2803219, fax: +90 216 2803404
* E-mail: zehra.sarac@medeniyet.edu.tr

Received: 10 April 2025 Revised: 30 June 2025 Accepted: 10 July 2025 Published:25 July 2025

Abstract: Fringe projection profilometry (FPP) is a three-dimensional imaging system and is widely used in object digitization, reverse engineering, etc. Therefore, it is important that FPP systems used for both research and commercial purposes are reliable. The random phase error that occurs is what affects the reliability of such a system the most. This error is not only caused by environmental noise, the geometry of the object being tested, etc. It also occurs due to the disadvantages of the methods used in the analysis of the data obtained from the system. For example, almost all methods are dependent on geometric shape, edge effects, value deviations, inability to see a large part of the object, shadow effects, etc., which cause problems. The aim of this study is to find a hybrid method based on Fourier transformation that is least affected by this randomly occurring phase noise, i.e., to identify the analysis method that least affects the reliability of the system. To do this, repeatability values obtained from the standard deviation calculated from the results obtained for each analysis method from the experimental data were used. As a result, it was determined that the 2D-EMD-FFT method, which gives the highest repeatability value, i.e., the lowest average standard deviation, has the least effect on the reliability of the system.

Keywords: L-FPP, 2D-EMD-FFT, TFFT, Hybrid methods, Repeatability, Reliability.

1. Introduction

Fringe projection profilometry (FPP) is used in applications where three-dimensional imaging is widely used, such as digitization of objects, reverse engineering, etc. [1-7]. In the literature, the performance of such systems is determined by parameters such as reliability, speed, accuracy, and cost [8-10]. Among these, the reliability and accuracy of the system stand out. The first of these is directly affected by factors such as the components of the FPP system, the geometry and surface properties of the measured objects, and the methods used to analyze the data obtained from the system [8-10]. The methods used to process data obtained from these systems generate random noise, producing an error known in the literature as phase error, which reduces the reliability of the system [11-14].

Signal analysis methods used in FPP imaging systems are generally divided into two categories:

Real-time methods: This is used for methods where data is processed at the moment it is collected or with very little delay.

Post-processing methods: These refer to analysis and processing methods performed offline after all data has been collected.

There are many studies in the literature on fringe analysis methods used in FPP systems [15-21].

In this study, several hybrid methods based on Fast Fourier Transform (FFT) that allow real-time fringe analysis were used. These can be listed as follows: (1) Traditional FFT (TFFT) (2) Savitzky-Golay Filtered FFT (SG-FFT) (3) Gaussian Window FFT (WFT) (4) 2D Empirical Mode Decomposition FFT (2D-EMD-FFT) ve (5) Modulated FFT (GPM-FFT). Previously, studies on accuracy have been conducted

using these methods in the L-FPP system through simulation and experimentation [12, 22]. In this study, the reliability of the system is investigated by calculating the repeatability parameter. In particular, determining the resistance of FPP systems to calibration errors, environmental effects, and optical aberrations in industrial applications requiring high sensitivity is of great importance in terms of the standardizability of the method. Therefore, the repeatability performance of L-FPP systems was evaluated through systematic experiments, and the results were compared with similar studies in the literature.

To date, there have been several studies in the literature on the reliability of the FPP system [26-30]. However, in these studies, repeatability was not evaluated using fringe analysis methods, but was only related to system error. In pioneering studies conducted by Zhang and Huang (2006), the sensitivity of phase-shifted FPP systems to systematic calibration errors was analyzed, and it was shown that accurate calibration significantly improved repeatability [23]. Later, Yoon and friends (2014) quantitatively evaluated the short-term repeatability of an FPP system through multiple measurements at different projection distances. In this study, measurement variation was analyzed using statistical metrics such as standard deviation and mean absolute difference, and it was reported that the system provided repeatability at the ±50 μm level [24]. Another important study was conducted by Wang et al. (2020). In this study, both the short-term and long-term repeatability of the FPP system were evaluated; In addition, the effect of environmental parameters such as temperature changes, lighting conditions, and projection angle on measurement accuracy has been systematically investigated. The authors have demonstrated that the long-term reliability of the system can be maintained above 98 % (e.g., 20 um at 1 mm) with appropriate environmental compensation strategies [25]. In 2023, Dong et al. proposed an easy-to-apply calibration method based on the RANSAC algorithm to improve measurement accuracy in fringe projection systems. This method improves accuracy by eliminating phase error data and does not require additional hardware. Experiments conducted on the double-sphere standard have shown that the standard deviation can be kept below 50 micrometers, especially in multiple measurements, this also demonstrates the stability and reliability of the method. In addition, measurement accuracy has been improved by up to 44 % compared to traditional methods [26].

In 2025, Wang et al. Multiple measurements with the SSSR-FPP (Single Shot Super-Resolved-SSSR) FPP system showed that the system provides high reproducibility. In repeated measurements using certified measurement standards (two ceramic spheres), the error values obtained for the radius and center-to-center distance (57.34 μm and 77.74 μm RMS error) are quite low. These low deviations demonstrate that the system can repeat measurements in a stable and reliable manner. In addition, similar accuracy was maintained in measurements taken at different time intervals of the ping-pong ball in free fall. This proves that the system is capable of repeatable measurements not only under static but also under dynamic conditions [27].

In this study, the question of whether the system is reliable is presented through repeatability derived from height values calculated using hybrid fringe analysis methods that generate random phase errors. The L-FPP system has been calibrated using the cross-sectional calibration method to obtain the specified height values [22]. In the study, white plaster sea horse and shell were used for measurements. Three measurements were taken at specific intervals for the sea horse and then the seashell before the calibrated system. These measured and reference fringe patterns were analyzed using the five hybrid methods mentioned above. Three-dimensional calibration section height values were obtained using five methods for each of the three measurements. Repeatability (standard deviation) values were calculated using these values. It will be determined that the method that gives the smallest mean standard deviation significantly improves the reliability of the system.

As a result, the 2D-EMD-FFT hybrid method provided the lowest average standard deviation for both objects. Therefore, it has been determined that this method is the most insensitive to noise, least affected by the measured object, etc., and increases the reliability of the system.

The article summarizes the hybrid methods used in Section 2, presents the experimental studies and results obtained in Section 3, and provides the general findings and discussions in Section 4.

2. Hybrid Fringe Analysis Methods Used in L-FPP Systems

The Fringe Projection system with Laser Projector (L-FPP) is shown in Fig. 1. This system gives the Fringe Pattern, which equals to Equation (1). Now it is presented each hybrid method shortly. First of all, Traditional Fourier Transform Method-TFFT is explained. After that, it is presented every method, respectively: FFT with Savitzky-Golay Filter (SG-FFT) (3) FFT with Gauss Window (WFT) (4) FFT with 2D Empirical Mode Decomposition (2D-EMD-FFT) and (5) FFT with Modulation (GPM-FFT).

$$i(x, y) = a(x, y) + b(x, y) \cos(2\pi f o x + + \phi(x, y)) \quad (1)$$

In the equation, *a, b* are the background intensity and the amplitude, respectively. ϕ is the phase containing information about the measured 3-D profile.

2.1. Traditional Fourier Transform Method-TFFT

Takeda and et.al. used the TFFT in 1982 to analyze the fringe pattern [28]. According to this method, if the Fast Fourier transform of Equation (1) is taken with respect to x, Equation (2) is obtained.

$$I(f,y) = A(f,y) + C(f - f_0,y) + \\ +C^*(f + f_0,y) \quad (2)$$

where f is the spatial frequency in the x direction. C^* is complex conjugate of the C. Here, if a bandpass filter with transfer function $H(f - f_0,y)$ is used, the component $C(f - f_0,y)$ is obtained from $I(f,y)$. If the inverse FFT of this operation is taken, the phase information (see Equation (3)) that gives the 3-D image of the object is obtained.

$$\phi(x,y) = \\ = arctan\frac{Im\{ifft[H(f-f_0,y)I(f,y)]\}}{Re\{ifft[H(f-f_0,y)I(f,y)]\}} \quad (3)$$

The discontinuous phase ϕ(x,y) is converted to a continuous form (unwrap operation) and the values of θ(x,y) are obtained. 3-B images are obtained using the fringe patterns obtained when the object is present and absent, θ_o and θ_{ref} are obtained in sequence. The difference between these $\Delta\theta = \theta_o - \theta_{ref}$ is used to calculate the height values, z.

$$\Delta\theta = \theta_o - \theta_{ref}, \quad (4)$$

$$z(x,y) = M\frac{L.p_0.(\frac{\Delta\theta(x,y)}{2\pi})}{p_0.(\frac{\Delta\theta(x,y)}{2\pi})-d} \quad (5)$$

Here, M is the calibration coefficient and is obtained using cross-sectional calibration [22]. Here, p_0 is the fringe period and can be found in [22]. L and d are shown in Fig. 1.

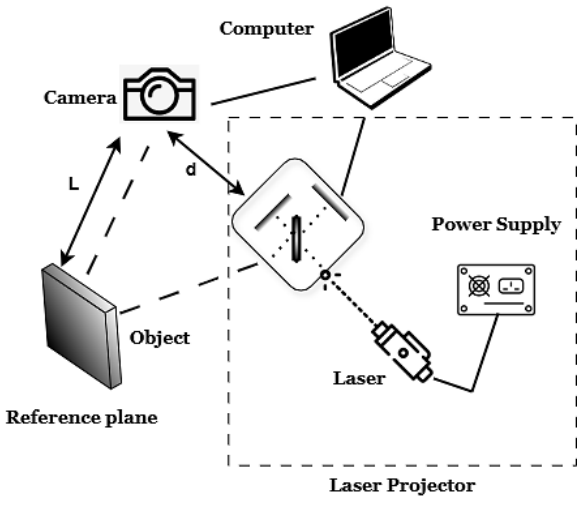

Fig. 1. L-FPP System.

2.2. Savitzky-Golay Filtered FFT (SG-FFT)

This filtering method was investigated in 1964 by Abraham Savitzky and Marcel J. E. Golay [29-31]. It is a simplified method for calculating the discrimination and smoothing of data with the least squares technique. In this method, after SG Filtering, inverse FFT is applied. The phase is obtained by (6)

$$\phi(x,y) = arctan\frac{Im\{ifft[SG(f-f_0,y)I(f,y)]\}}{Re\{ifft[SG(f-f_0,y)I(f,y)]\}} \quad (6)$$

These discontinuous phase values are unwrapped to obtain continuous phase values $\theta(x,y)$. The phase difference and height values are obtained by Equation (4) and (5), respectively.

2.3. Gaussian Window FFT (WFT)

This study also uses the Gauss windowed FFT method, which is widely known in the literature [32-33].

Equation (1) shows that the fringe pattern consists of background intensity and two exponential functions. This pattern has three spectrum components in the frequency domain. The WFT of the signal in (1) can be written as follows.

$$i(x) = \frac{1}{2\pi}\int_{-\infty}^{+\infty}\left\{\begin{matrix}[i(x)\otimes h(x,f)]\otimes \\ \otimes h(x,f)\end{matrix}\right\} df, \\ i(x) = \frac{1}{2\pi}\int_{-\infty}^{+\infty}\left\{\begin{matrix}[i(x)\otimes h(x,f)]\otimes \\ \otimes h(x,f)\end{matrix}\right\} df, \quad (6) \\ h(x,f) = g(x)exp(jfx), \\ g(x) = exp(-\frac{x^2}{2\sigma^2}),$$

where ⊗ shows the convolution. If $i(x)\otimes h(x,f)$ is less than a certain value, it behaves like noise. Therefore, it is important to determine this specific (threshold) value. Therefore, the integral is taken over a region (between a and b) with a Gauss window width in a limited interval. Thus, if the WFT of the fringe pattern is taken, (8) is obtained.

$$\widetilde{\imath(x)} = \frac{1}{2\pi}\int_a^b\left\{\begin{matrix}[i(x)\otimes h(x,f)]\otimes \\ \otimes h(x,f)\end{matrix}\right\} df \quad (8)$$

In this case, the 2D phase can be written as follows (9).

$$\phi(x,y) = arctan\frac{Im\{\widetilde{\imath(x)}\}}{Re\{\widetilde{\imath(x)}\}} \quad (9)$$

These $\phi(x,y)$ values are unwrapped to obtain continuous phase values, $\theta(x,y)$. The difference and height values between the obtained θ_o ve θ_{ref} phases for the image taken with the reference image and object are calculated using (4) and (5).

2.4. 2D Empirical Mode Decomposition FFT (2D-EMD-FFT)

2D-EMD is a nonlinear and adaptive decomposition method used to decompose an image (two-dimensional signal) into its different frequency components (detail levels) [12]. 1D EMD was developed by Huang et al. to analyze time series (e.g., audio signals) [34]. This method splits the signal into a bunch of Intrinsic Mode Functions (IMFs) and a residual component. 2D-EMD applies this logic to images.

The fringe pattern i(x,y) given by equation (10) is decomposed into IMF's and a residual component as follows:

$$i(x,y) = \sum_{k=1}^{n} IMF_k(x,y) + r_n(x,y), \quad (10)$$

where $IMF_k(x,y)$: k. IMF component (partial frequency content), $r_n(x,y)$: residual component (background, noise, etc.).

$IMF_k(x,y)$ values obtained when there is no object (reference) and when there is an object are obtained. It is collected and given as a noiseless fringe pattern (11).

$$\widehat{i(x,y)} = \sum_{k=1}^{n} IMF_k(x,y) \quad (11)$$

From here on, phase acquisition is done using TFFT. That is, the FFT of (11) is taken with respect to x and $\widehat{I(f,y)}$ is found. From there after filtering the discontinuous phase (12) is obtained.

$$\phi(x,y) = arctan\frac{Im\left\{ifft\left[H(f-f_0,y)\widehat{I(f,y)}\right]\right\}}{Re\{ifft[H(f-f_0,y)\widehat{I(f,y)}]\}} \quad (12)$$

These ϕ(x,y) values are unwrapped to obtain the continuous phase values θ(x,y). The difference and height values from the θ_o ve θ_{ref} phases are found with (4) and (5).

2.5. Modulated FFT (GPM-FFT)

In this method, the modulation process is performed by multiplying the fringe pattern i(x,y) given in (1) with the Gaussian window g(x,y) as follows [12].

$$m(x,y) = i(x,y)g(x,y) \quad (13)$$

Then the steps in the TFFT method are followed. That is, the FFT of m(x,y) with respect to x is obtained $M(f,y)$. The result is multiplied by the band pass filter and the phase found with the inverse FFT is given as in (14).

$$\phi(x,y) = = arctan\frac{Im\{ifft[H(f-f_0,y)M(f,y)]\}}{Re\{ifft[H(f-f_0,y)M(f,y)]\}} \quad (14)$$

The $\phi(x,y)$ obtained for the images obtained with and without an object consists of the phase values between –π and +π. To make this phase continuous, a suitable unwrap algorithm is used to reach continuous phase values $\theta(x,y)$. The difference and height values from the θ_o ve θ_{ref} phases are found with (4) and (5).

3. Experimental Studies and Results

The 3-D images of the seashell and horse used in this study (see Fig. 2 and 4) were obtained using the L-FPP system. To determine the reliability of the system, three measurements were taken at random times on the same day for each object, and the results were evaluated using each hybrid analysis method.

In this study, a vertical section calibrated using the cross-sectional calibration method was found [22]. In the reliability study, only calibrated vertical sections obtained by dividing each object in half were used. The 3-D results showing the cross sections obtained from the sea horse body using hybrid analysis methods for the second measurement are presented in Fig. 2. The vertical sections taken in this manner are marked in blue. The same sections were used in other measurements as well.

The time intervals at which repeated measurements were taken for the sea horse are presented in Table 1.

Table 1. Measurements taken for the seahorse.

Seahorse	1st Measurement t = 0 s	2nd Measurement	3rd Measurement
Time between measurements (s)	0 s	51 s	120 s

The superimposed drawings of the sections obtained from the three measurements in the table are shown in Fig. 3.

The standard deviations (σ) obtained for each point of the section from these measurements were calculated (see (15)) and the average standard deviation $\bar{\sigma}$, a parameter indicating the repeatability of the system, was found as in equation (16).

$$\sigma = \sqrt{\frac{1}{n}\sum_{i=1}^{n}(z_i - \bar{z})^2} \quad (15)$$

Here, n is taken as the length of the vertical section, z is taken as the height values, and $\bar{z}$ is taken as the average height value. It is calculated separately for each hybrid method.

Then, the average of all standard deviation values found is calculated as follows.

$$\bar{\sigma} = \frac{1}{n}\sum_{i=1}^{n}\sigma_i \quad (16)$$

These values, which indicate the reliability of the system, have been calculated for each hybrid method, and the results found for the sea horse are presented in Table 2.

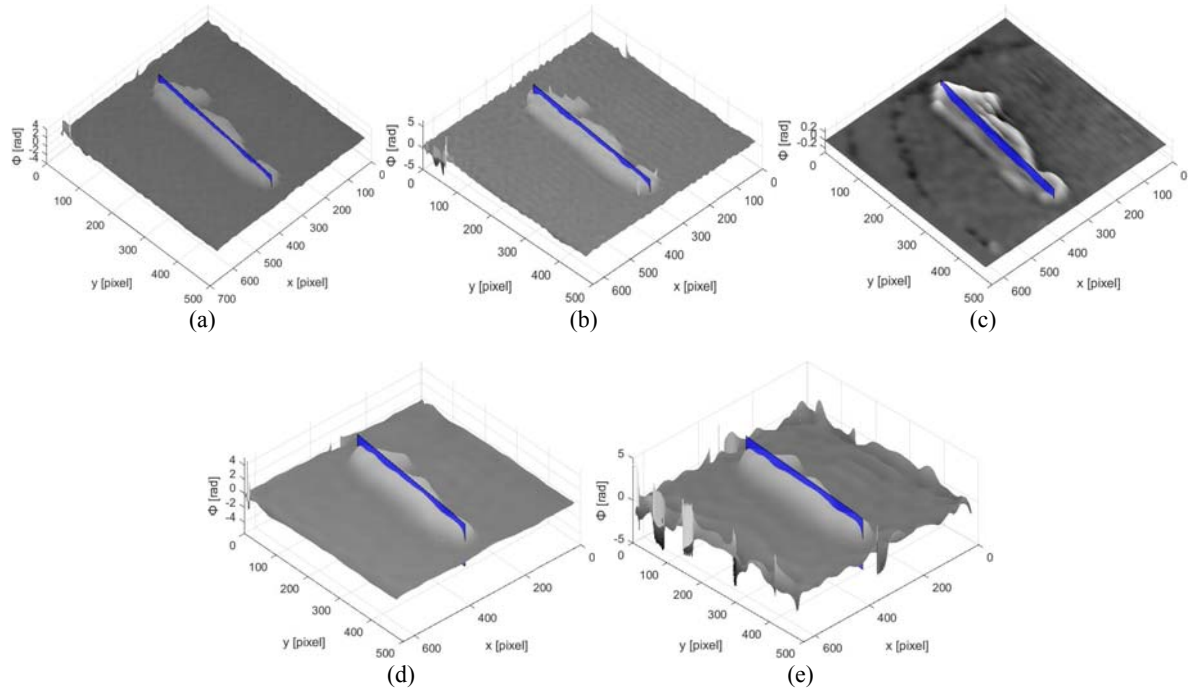

Fig. 2. 3-D images obtained using hybrid methods from the second measurement results obtained from the system for the Seahorse object in Table 1. Here, the section where the height values are calculated is shown in blue. 3-D Images obtained Fig. 2. (a) with 2D EMD FFT, (b) with SG FFT, (c) with WFT, (d) with TFFT and (e) GPM FFT.

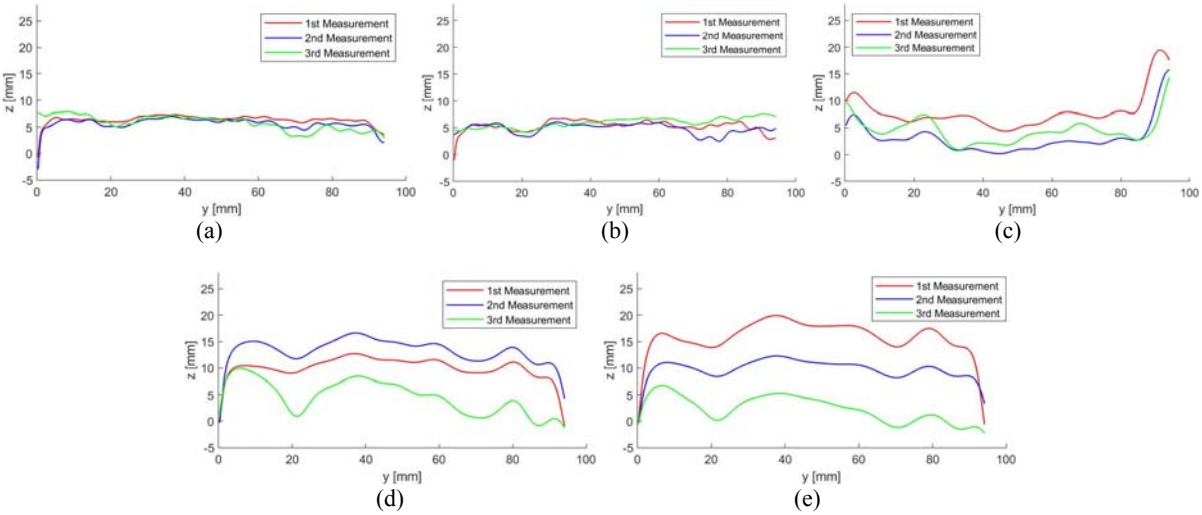

Fig. 3. Sections obtained from the Seahorse body using hybrid methods for three measurements taken from the L-FPP system at the time intervals given in Table 1. Sections obtained with (a) 2D EMD FFT, (b) SG FFT, (c) WFT, (d) TFFT, and (e) GPM FFT.

Table 2. Mean standard deviation values expressing repeatability obtained from three measurements made with the Seahorse.

Hybrid Method	Mean Standard Deviation (mm)
TFFT	4.65106
SG-FFT	0.72649
WFT	2.53096
2D-EMD-FFT	**0.60906**
GPM-FFT	7.12001

The reliability of the system was also investigated through repeated measurements of seashell. Three consecutive measurements were taken. The time intervals at which the repeated measurements were taken are presented in Table 3.

The 3-D phase maps obtained with each method for the second measurement with the seashell are shown in Fig. 4. This is a vertical section showing the height values indicated in blue in the figure. This section is also used in other measurements.

Table 3. Measurements taken for the seashell

Seashell	1st Measurement t = 0 s	2nd Measurement	3rd Measurement
Time between measurements (s)	0 s	40 s	80 s

The superimposition of the sections obtained by evaluating the measurement results obtained at specific time intervals from the L-FPP system with each hybrid method is shown in Fig. 5.

The average standard deviation values calculated using the sections in these figures are presented in Table 4. Which hybrid method ensures the reliability of the L-FPP system? The answer to this question can be found in Tables 2 and 4. The 2D-EMD-FFT hybrid method, which gives the smallest standard deviation value in the tables, is the most reliable method.

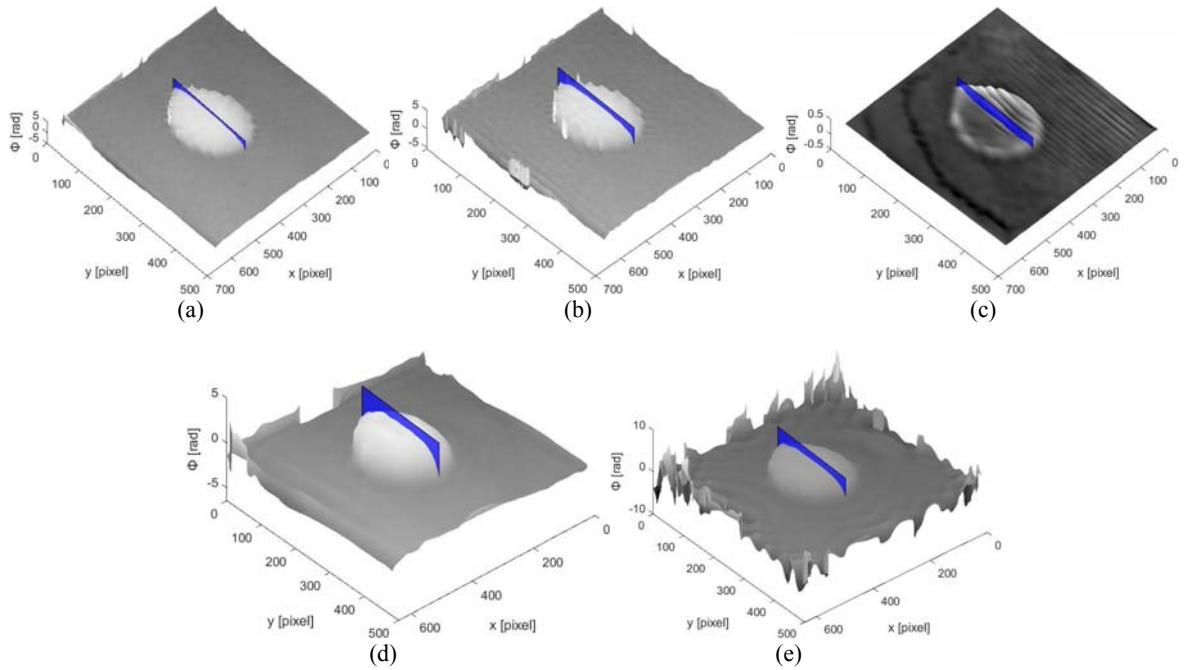

Fig. 4. 3-D images obtained using hybrid methods from the second measurement results obtained from the system for the Seashell object in Table 3. Here, the section where the height values are calculated is shown in blue. 3-D Images obtained Fig. 4. (a) with 2D EMD FFT, (b) with SG FFT, (c) with WFT, (d) with TFFT and (e) GPM FFT

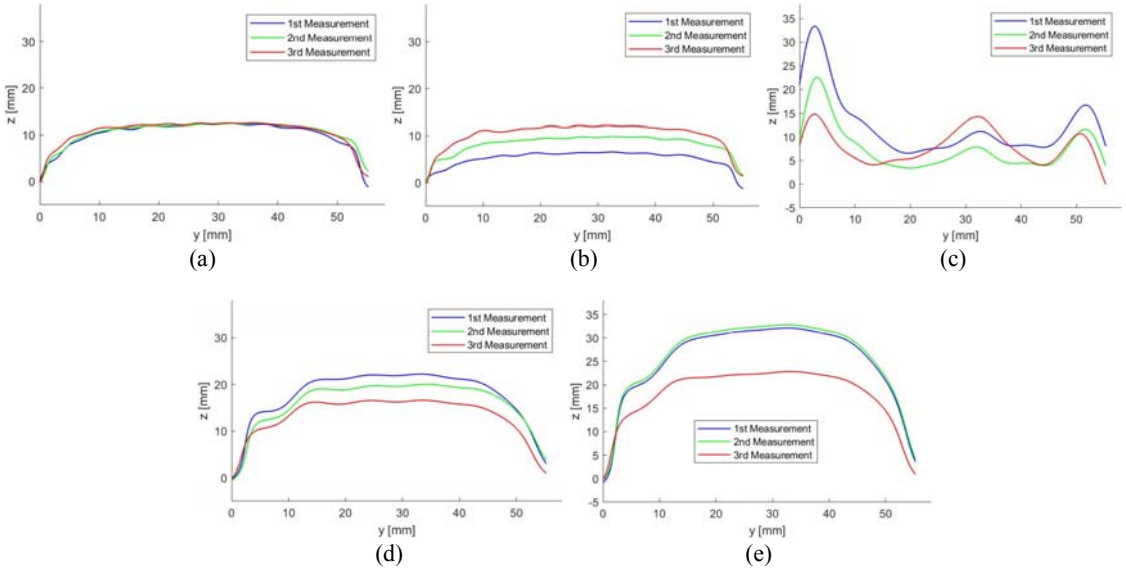

Fig. 5. Sections obtained from the Seashell body using hybrid methods for three measurements taken from the L-FPP system at the time intervals given in Table 3. Sections obtained with (a) 2D EMD FFT, (b) SG FFT, (c) WFT, (d) TFFT, and (e) GPM FFT.

4. Results and Discussion

In this study, the reliability of the laser projector-based FPP system is investigated using several hybrid methods based on Fast Fourier Transform (FFT) that allow real-time fringe analysis. These methods can be listed as follows: (1) Traditional FFT (TFFT) (2) Savitzky-Golay Filtered FFT (SG-FFT) (3) Gaussian Window FFT (WFT) (4) 2D Empirical Mode Decomposition FFT (2D-EMD-FFT) and (5) Modulated FFT (GPM-FFT). The aim is to determine how these methods affect the reliability of the system. Here, the repeatability parameter for the reliability test is given by the average standard deviation.

Table 4. Mean standard deviation values expressing repeatability obtained from three measurements made with the Seashell.

Hybrid Method	Mean Standard Deviation (mm)
TFFT	2.52157
SG-FFT	2.77314
WFT	2.65934
2D-EMD-FFT	**0.20600**
GPM-FFT	4.98470

In the study, measurements were taken using plaster casts of sea horse and shell. Three measurement results were obtained from the system at different times for both objects. The height values obtained using the vertical section derived from these measurement results were evaluated in terms of how they follow each other and overlap, and standard deviations were calculated.

The mean standard deviation values calculated from the height values for seahorse and seashell are presented in Tables 2 and 4, respectively. When calculating the standard deviations, a total of 200 pixels were omitted from the beginning and end of the cross-section in order to exclude edge effects caused by the methods.

Looking at Table 2, where the results obtained for seahorse are presented, the 2D-EMD-FFT method gives the best average standard deviation. This gives a repeatability of about 39 %, followed by the SG-FFT method with 27 %. The reproducibility offered by other methods is quite low, i.e. it evolves to 0 % and becomes negative.

Looking at Table 4, which presents the results obtained for Seashell, the 2D-EMD-FFT method gives the best average standard deviation. This value offers a repeatability of about 79 %, followed by the TFFT method with a negative percentage. The reproducibility, i.e. the average standard deviation, offered by other methods is also quite low.

As a result, it can be said that the 2D-EMD-FFT method is the most stable method. Because it is the method that is least affected by random phase noise and is more successful in obtaining the same result from the system in all time. As for the other methods; first of all, it was observed that the SG filter used for the SG-FFT method needs correction on its parameters for each measurement. Depending on the effect of this filter, the average standard deviation value it gives also changes, so it was determined that it is the 4th method that makes the system the most reliable for seashell, while it ranks 2nd for seahorse. As for the TFFT method, it was found to be the 4th method for the seahorse and the 2nd method for the seashell due to its disadvantages such as the extra edge effect and its inability to deal with random noise.

The interpretation made for SG-FFT can also be made for WFT and GPM FFT. This is because these methods also use a Gaussian window and these windows are chosen with different widths for each object. Therefore, it is clear that these methods exhibit instability and therefore affect the reliability of the system too much.

As a result, it is concluded that the fringe analysis method that increases the reliability of the L-FPP system is the 2D-EMD-FFT hybrid method, which is the most stable method and shows the lowest average standard deviation, i.e. repeatability value.

This result is in line with the group's previous studies on the accuracy of the L-FPP system. In this study, a comparison with the studies in the literature could not be made. Because no study has been identified that performs a repeatability test with fringe analysis methods.

References

[1]. Z. Chen, M. Zhu, C. Sun, Y. Liu, et al., Fringe projection profilometry for three-dimensional measurement of aerospace blades, *Symmetry*, Vol. 16, Issue 3, 2024, 350.

[2]. D. P. K. Lun, Y. -H. Chan, Robust single-shot fringe projection profilometry based on morphological component analysis, *IEEE Transactions on Image Processing*, Vol. 27, Issue 11, 2018, pp. 5393-5405.

[3]. S. V. der Jeught, J. J. J. Dirckx, Real-time structured light profilometry: a review, *Optics and Lasers in Engineering*, Vol. 87, 2016, pp. 18-31.

[4]. S. Zhang, High-speed 3D shape measurement with structured light methods: a review, *Optics and Lasers in Engineering*, Vol. 106, 2018, pp. 119-131.

[5]. M. d. C. Casas Pérez, G. Moreno Chávez, F. Castillo Rivera, D. Sarocchi, et al., Fringe projection method for 3D high-resolution reconstruction of oil painting surfaces, *Heritage*, Vol. 6, 2023, pp. 3461-3474.

[6]. A. G. Marrugo, F. Gao, S. Zhang, State-of-the-art active optical techniques for three-dimensional surface metrology: a review, *Journal of the Optical Society of America A*, Vol. 37, Issue 9, 2020, pp. B60-B77.

[7]. G. Zhang, Y. Liu, Q. Yao, H. Deng, et al., Multi-view fringe projection profilometry for surfaces with intricate structures and high dynamic range, *Optics Express*, Vol. 32, Issue 11, 2024, pp. 19146-19162.

[8]. H. Nguyen, J. Liang, Y. Wang, A. Wang, Accuracy assessment of fringe projection profilometry and digital image correlation techniques for

three-dimensional shape measurements, *Journal of Physics: Photonics*, Vol. 1, Issue 3, 2019, 014004.
[9]. S. Zhang, T. Su, F. Gao, C. Shi, et al., DOE-based structured-light method for accurate 3D sensing, *Optics and Lasers in Engineering*, Vol. 120, 2019, pp. 21-30.
[10]. J. Wang, Z. Zhang, R. K. Leach, W. Lu, et al., Predistorting projected fringes for high-accuracy 3-D phase mapping in fringe projection profilometry, *IEEE Transactions on Instrumentation and Measurement*, Vol. 70, 2021, 1500309.
[11]. B. Li, C. Tang, X. Zhu, Y. Su, et al., Shearlet transform for phase extraction in fringe projection profilometry with edges discontinuity, *Optics and Lasers in Engineering*, Vol. 78, 2016, pp. 91-98.
[12]. B. Özbay, Z. Saraç, Inspection of the accuracy of fringe projection profilometry by using hybrid methods, *NOHU Journal of Engineering Sciences*, Vol. 13, Issue 4, 2024, pp. 1452-1467.
[13]. L. Huang, Q. Kemao, B. Pan, A. K. Asundi, Comparison of Fourier transform, windowed Fourier transform, and wavelet transform methods for phase extraction from a single fringe pattern in fringe projection profilometry, *Optics and Lasers in Engineering*, Vol. 48, 2010, pp. 141-148.
[14]. X. Li, Z. Zhang, C. Yang, Reconstruction method for fringe projection profilometry based on light beams, *Applied Optics*, Vol. 55, Issue 34, 2016, pp. 9895-9906.
[15]. K. Yan, H. Tian, E. Liu, R. Zhao, et al., A decoupled calibration method for camera intrinsic parameters and distortion coefficients, *Mathematical Problems in Engineering*, Vol. 2016, 2016, 2075670.
[16]. J. Lu, R. Mo, H. Sun, Z. Chang, Flexible calibration of phase-to height conversion in fringe projection profilometry, *Applied Optics*, Vol. 55, Issue 23, 2016, pp. 6381-6389.
[17]. Y. Xiao, J. Liu, H. Zhong, Flexible calibration for digital fringe projection profilometry, in *Proceedings of the IEEE International Conference on Mechatronics and Automation (ICMA'14)*, 2014, pp. 1855-1860.
[18]. Z. Zhang, A flexible new technique for camera calibration, *IEEE Transactions on Pattern Analysis and Machine Intelligence*, Vol. 22, Issue 11, 2000, pp. 1330-1334.
[19]. S. Lv, D. Tang, X. Zhang, D. Yang, et al., Fringe projection profilometry method with high efficiency, precision, and convenience: theoretical analysis and development, *Optics Express*, Vol. 30, Issue 19, 2022, pp. 33515-33537.
[20]. H. Yue, B. Zhao, Y. Wu, M. Li, Flexible global calibration technique for an arbitrarily arranged fringe projection profilometry system, *Optical Engineering*, Vol. 55, Issue 6, 2016, 064113.
[21]. P. S. Huang, Novel method for structured light system calibration, *Optical Engineering*, Vol. 45, Issue 8, 2006, 083601.
[22]. B. Özbay, Z. Saraç, Experimental investigation of the accuracy of profilometry with laser projector, in *Proceedings of the 8th International Conference on Optics, Photonics and Lasers (OPAL'25)*, 2025, pp. 15-22.
[23]. S. Zhang, P. S. Huang, High-resolution, real-time 3D shape measurement, *Optical Engineering*, Vol. 45, Issue 12, 2006, 123601.
[24]. J. Yoon, J. H. Lee, J. Park, Quantitative repeatability evaluation of fringe projection profilometry system for micro-feature measurement, *Measurement Science and Technology*, Vol. 25, Issue 3, 2014, 035202.
[25]. Y. Wang, X. Liu, Y. Wang, Repeatability and environmental robustness of fringe projection profilometry: experimental evaluation and compensation strategy, *Optics and Lasers in Engineering*, Vol. 134, 2020, 106281.
[26]. G. Dong, X. Sun, L. Kong, X. Peng, Suppression for phase error of fringe projection profilometry using outlier-detection model: development of an easy and accurate method for measurement, *Photonics*, Vol. 10, 2023, 1252.
[27]. B. Wang, W. Chen, J. Qian, S. Feng, et al., Single-shot super-resolved fringe projection profilometry (SSSR-FPP): 100,000 frames-per-second 3D imaging with deep learning, *Light: Science & Applications*, Vol. 14, 2025, 70.
[28]. M. Takeda, K. Mutoh, Fourier transform profilometry for the automatic measurement of 3D object shapes, *Applied Optics*, Vol. 22, Issue 24, 1983, pp. 3977-3982.
[29]. A. Savitzky, M. J. E. Golay, Smoothing and differentiation of data by simplified least squares procedures, *Analytical Chemistry*, Vol. 36, Issue 8, 1964, pp. 1627-1639.
[30]. P. A. Gorry, General least-squares smoothing and differentiation by the convolution (Savitzky-Golay) method, *Analytical Chemistry*, Vol. 62, Issue 6, 1990, pp. 570-573.
[31]. M. A. Awal, S. S. Mostafa, M. Ahmad, Performance analysis of Savitzky-Golay smoothing filter using ECG signal, *International Journal of Computer and Information Technology*, Vol. 1, Issue 2, 2011, p. 24.
[32]. Q. Kemao, Two-dimensional windowed Fourier transform for fringe pattern analysis: principles, applications and implementations, *Optics and Lasers in Engineering*, Vol. 45, 2007, pp. 304-317.
[33]. Q. Kemao, Windowed Fourier transform for fringe pattern analysis, *Applied Optics*, Vol. 43, Issue 13, 2004, pp. 2695-2702.
[34]. N. E. Huang, Z. Shen, S. R. Long, et al., The empirical mode decomposition and the Hilbert spectrum for nonlinear and non-stationary time series analysis, *Proceedings of the Royal Society of London. Series A: Mathematical, Physical and Engineering Sciences*, Vol. 454, 1998, pp. 903-995.